Bioconjugate Chemistry

Article

pubs.acs.org/bc

Cholesterol-Based Nucleolipid-Ruthenium Complex Stabilized by Lipid Aggregates for Antineoplastic Therapy

Luca Simeone,[†] Gaetano Mangiapia,[‡,∥] Giuseppe Vitiello,[‡,∥] Carlo Irace,[§] Alfredo Colonna,[§] Ornella Ortona,[‡,∥] Daniela Montesarchio,*[,†] and Luigi Paduano*[,‡,∥]

[†]Dipartimento di Chimica Organica e Biochimica, [‡]Dipartimento di Chimica "Paolo Corradini", Università "Federico II" di Napoli, Complesso Universitario di Monte S. Angelo, via Cintia, 4, 80126 Naples, Italy

[∥]CSGI – Consorzio interuniversitario per lo sviluppo dei Sistemi a Grande Interfase

[§]Dipartimento di Farmacologia Sperimentale, Università "Federico II" di Napoli, via D. Montesano 49, 80131 Naples, Italy

Supporting Information

ABSTRACT: A novel ruthenium complex, linked to a cholesterol-containing nucleolipid (named ToThyCholRu), stabilized by lipid aggregates for antineoplastic therapy is presented. In order to retard the degradation kinetics typically observed for several ruthenium-based antineoplastic agents, ToThyCholRu is incorporated into a liposome bilayer formed by POPC. The resulting nanoaggregates contain up to 15% in moles of the ruthenium complex, and are shown to be stable for several weeks. The liposomes host the ruthenium–nucleolipid complex with the metal ion surrounded by POPC lipid headgroups and the steroid moiety inserted in the more external acyl chain region. These ruthenium-containing liposomes are more effective in inhibiting the growth of cancer cells than a model NAMI-A-like ruthenium complex, prepared for a direct evaluation of their antiproliferative activity. These results introduce new perspectives in the design of innovative transition-metal-based supramolecular systems for anticancer drug vectorization.

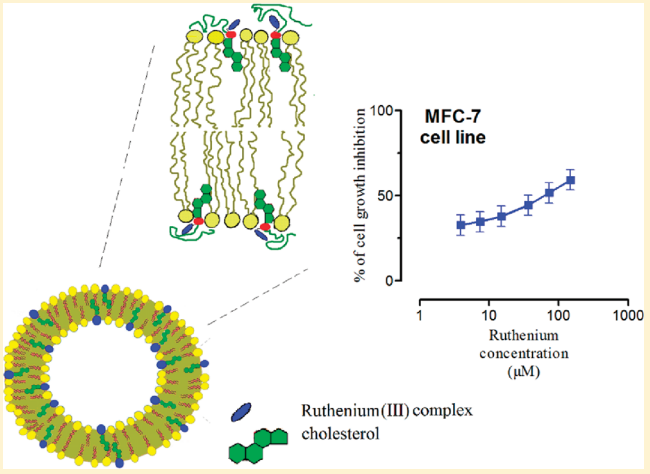

INTRODUCTION

In the past three decades, a number of ruthenium-based drugs have been proposed as antineoplastic agents, and some of them have been successfully tested for potential antitumor activity.[1] In several cases, the design of these compounds was largely inspired by well-known Pt complexes. Indeed, Cisplatin is still the most widely used chemotherapeutic drug for the treatment of several malignancies,[2,3] though its use is associated with severe side effects, and limited in many anticancer therapeutic protocols by primary and acquired resistance to it. These drawbacks have led to exploration of other transition metal complexes as efficient alternatives to Pt-based agents. Osmium, ruthenium, and titanium complexes offer some very interesting examples.[4]

As confirmed by the large number of papers appearing in the literature in the last two decades, ruthenium complexes have emerged as the most promising alternatives to Pt-based antineoplastic agents in biological screenings. Since the early 1980s, Sava and co-workers have been pioneers in studying the perspectives of transition-metal complexes, developing, among others, the ruthenium complex named NAMI-A, found to be a very active anticancer agent in *in vitro* assays. This compound, along with KP1019 and RAPTA-C, has reached human clinical testing and has completed Phase I clinical trials.[5]

Even if a large number of studies on Ru complexes have been published in recent years, to the best of our knowledge the unique example of nanovector-carrying ruthenium complexes for anticancer therapy has been reported by some of us only.[6−8]

As is well-known, amphiphilic self-assembly allows an efficient bottom-up strategy in order to obtain nanosized aggregates whose volume and shape are quite easily tunable. The incorporation of appropriate complex structural motifs in suitable amphiphilic building blocks, used as starting monomers, may lead to functional aggregates of great interest in the development of novel smart materials, with applications in both nanotechnology and nanomedicine. In this framework, with the aim of obtaining efficient delivery and controlled release of anticancer agents, we recently synthesized a new nucleolipid-based ruthenium complex that spontaneously incorporates into the phospholipid membrane of a liposome. As an evolution of

Received: October 31, 2011
Revised: February 13, 2012
Published: February 28, 2012

   dx.doi.org/10.1021/bc200565v | *Bioconjugate Chem.* 2012, 23, 758–770

our previous work, we describe here the synthesis, molecular, and aggregation characterization along with bioactivity investigations of a novel cholesterol-containing ruthenium complex, baptized ToThyCholRu. This system has been studied as such and in parallel, when lodged in the biomimetic membrane formed by the naturally occurring lipid 1-palmitoyl-2-oleoyl-*sn*-glycero-3-phosphocholine, POPC.

Our purposes are to develop highly biomimetic liposomes able to preserve the bioactive ruthenium complex core from degradation and to deliver a higher amount of antineoplastic agent to the target cells, thus resulting into a more active anticancer drug.

By exploiting the high affinity of cholesterol with phospholipids, ToThyCholRu has been designed so to achieve easy penetration through the cell membrane, thus facilitating ruthenium complex internalization. This strategy has been successfully applied in the antisense strategy for gene therapy using oligonucleotides end-modified with a cholesterol motif. In fact, it has been observed that cholesterol conjugation to oligonucleotides results in high accumulation of the oligomers in various liver[9] and spleen cell types.[10]

Regarding the NAMI-A ruthenium complex, in spite of the quite encouraging clinical results, some questions are still open about its *in vivo* applicability, mainly due to its low stability in physiological conditions. In analogy with Cisplatin, the chloride ligands of the ruthenium complex are replaced by hydroxide ligands in a few hours. This leads to partial hydrolysis of the complex and to poly-oxo species formation.[11,12] Although it is guessed that the formation of poly-oxo species does not really alter the ruthenium activity, at least for some tumor cell lines,[13] as far as Cisplatin is concerned it has been shown that its premature aquation and hydrolysis in the extracellular medium deactivate up to 98% of the Pt complex administered. Thus, in order to drastically reduce the degradation process, our basic idea was to move *in vivo* ToThyCholRu using POPC-based liposomes as carrier. The ruthenium complex anchored to the cholesteryl−thymidine nucleolipid is incorporated by force into the liposome bilayer, in a region where the contact with water or hydroxy groups is reduced, thus sensibly retarding the degradation kinetics. The amphiphilic nanoaggregates described here contain up to 15 mol % ruthenium complex, which at this composition is stable for several weeks.

The study was carried out through the following steps: *(i)* synthesis of the Ru(III) complex, built on a thymidine scaffold incorporating the lipophilic cholesterol moiety and a hydrophilic polyoxyethylene chain; *(ii)* structural characterization of the aggregates generated by this complex, in the absence and in the presence of POPC; *(iii)* control of the stability of the Ru complexes in both forms; and *(iv)* antiproliferative *in vitro* investigations of the formulation.

The self-aggregation properties were studied by dynamic light scattering, DLS, and small-angle neutron scattering, SANS, whereas the degradation process was studied by UV−vis measurements and electron paramagnetic resonance, EPR. A limited panel of human tumor cell lines (HeLa cervical cancer cells, CaCo-2 and WiDr epithelial colorectal adenocarcinoma cells, MCF-7 breast adenocarcinoma cells, SH-SY5Y neuroblastoma cells) have been used to evaluate the cytotoxic activity of the Ru-containing aggregates.

MATERIALS AND METHODS

General Synthetic Methods. All the reagents were of the highest commercially available quality and were used as received. TLC analyses were carried out on silica gel plates from Merck (60, F254). Reaction products on TLC plates were visualized by UV light and then by treatment with a 10% $Ce(SO_4)_2/H_2SO_4$ aqueous solution. For column chromatography, silica gel from Merck (Kieselgel 40, 0.063−0.200 mm) was used.

1-Palmitoyl-2-oleoyl-*sn*-glycero-3-phosphocholine, POPC, from Avanti Polar and cholesterol, Chol, from Sigma, purity >99%, were used as received. Water used for liposome preparation was obtained by Millipore Elix 3 apparatus.

NMR spectra were recorded on Bruker WM-400, Varian Gemini 200, and Varian Inova 500 spectrometers, as specified. All the chemical shifts are expressed in ppm with respect to the residual solvent signal. Peak assignments have been carried out on the basis of standard H−H COSY and HSQC experiments. For the ESI MS analyses, a Waters Micromass ZQ instrument—equipped with an electrospray source—was used in the positive and/or negative mode. MALDI TOF mass spectrometric analyses were performed on a PerSeptive Biosystems Voyager-De Pro MALDI mass spectrometer in the linear mode using 3,4-dihydroxybenzoic acid as the matrix.

The NMR and MS characterization of ToThyCholRu and related synthetic intermediates are described in detail in the Supporting Information.

Synthesis. *Synthesis of 3-(4-Pyridylmethyl), 3′-O-Cholesteroxyacetyl, 5′-O-(4,4′-Dimethoxytriphenyl-methyl)-thymidine (**4**).* 5′-*O*-(4,4′-Dimethoxytriphenylmethyl)-thymidine **2** (396 mg, 0.73 mmol) was dissolved in 5 mL of dry DMF. K_2CO_3 (302 mg, 2.18 mmol) and 4-(bromomethyl)-pyridine hydrobromide (276 mg, 1.09 mmol) were sequentially added to the reaction mixture, left under stirring at 60 °C. After 12 h, TLC analysis indicated the presence of one main product in the reaction mixture. Alkylated compound **3** was not isolated, but directly converted into its 3′-conjugated derivative **4** (see Scheme 1). To this purpose, the solvent was removed and the residual solid was taken up in DCM, washed with water, dried over anhydrous Na_2SO_4, and concentrated in vacuo. Successively, the residue was dissolved in 3 mL of dry DCM, and then DMAP (32 mg, 0.266 mmol), cholesteroxy-acetic acid **8** (118 mg, 0.266 mmol), and DCC (55 mg, 0.266 mmol) were sequentially added. The reaction mixture was stirred for 12 h at room temperature, and then the solvent was removed in vacuo; the crude product was purified by chromatography on a silica gel column with *n*-hexane/AcOEt (1:1, v/v, containing 1% of TEA) as eluent, yielding the desired compound **4** in 19% yields for the two steps (144 mg, 0.14 mmol, unoptimized yield).

*Synthesis of 3-(4-Pyridylmethyl), 3′-O-Cholesteroxyacetyl Thymidine (**5**).* **4** (140 mg, 0.13 mmol) was dissolved in 3 mL of a 1% TCA solution in DCM and stirred for 1 h at room temperature (see Scheme 1). The reaction mixture was then concentrated in vacuo and purified by chromatography on a silica gel column with $CHCl_3/CH_3OH$ (99:1, v/v) as eluent, giving the desired compound **5** in almost quantitative yields (100 mg, 0.13 mmol).

*Synthesis of 3-(4-Pyridylmethyl), 3′-O-Cholesteroxyacetyl, 5′-O-Monomethoxy-triethylene Glycol Acetyl Thymidine (**6**, ToThyChol).* **5** (96 mg, 0.13 mmol) was dissolved in 2 mL of dry DCM, and then DMAP (46 mg, 0.38 mmol), carboxylic acid **10** (41 mg, 0.18 mmol), and DCC (38 mg, 0.18 mmol) were sequentially added (see Scheme 1). The reaction mixture was stirred for 12 h at room temperature and the solvent was then removed in vacuo; the crude product was purified by chromatography on a silica gel column with *n*-hexane/acetone

dx.doi.org/10.1021/bc200565v | *Bioconjugate Chem.* 2012, 23, 758−770

Scheme 1. Synthetic Scheme for the Preparation of Ruthenium Complex 1 (ToThyCholRu)[a]

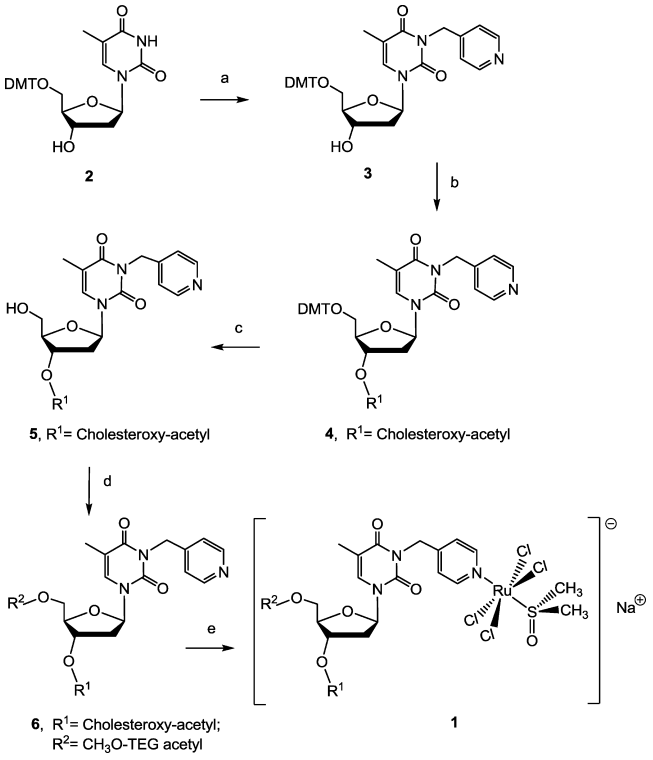

[a]Reaction conditions: (a) 4-(bromomethyl)pyridine, K_2CO_3, DMF, 12 h, 60 °C; (b) cholesteroxy acetic acid (**8**), DCC, DMAP, CH_2Cl_2, 12 h, r.t.; (c) 1% TCA in CH_2Cl_2, 1 h, r.t.; (d) CH_3O-TEG acetic acid (**10**), DCC, DMAP, CH_2Cl_2, 4 h, r.t.; (e) [trans-$RuCl_4(DMSO)_2$]$^-$ Na^+, CH_3CN, 4 h, 50 °C.

(1:1, v/v) as eluent, giving the desired compound **6** in 85% yields (106 mg, 0.11 mmol).

*Synthesis of tert-Butyl Cholesteroxy-Acetate (**7**).* Cholesterol (963 mg, 2.5 mmol) was dissolved in 4 mL of dry THF, and NaH 60% p.p. (200 mg, 4.98 mmol) and then *t*-butyl bromoacetate (920 μL, 6.22 mmol) were sequentially added to the reaction mixture taken at 0 °C. After 24 h at room temperature, the reaction was quenched by addition of CH_3OH (2 mL) and the solvent removed in vacuo (see Scheme 2). The residual solid was taken up in DCM, washed with water, dried over anhydrous Na_2SO_4, and concentrated in vacuo. The residue was then purified by chromatography on a silica gel column using *n*-hexane/AcOEt (9:1, v/v) as eluent, yielding the desired compound **7** in 31% yield (392 mg, 0.77 mmol).

*Synthesis of Cholesteroxy-Acetic Acid (**8**).* Ester **7** (300 mg, 0.59 mmol) was dissolved in 3.0 mL of formic acid and stirred at room temperature for 2 h. The solvent was then removed in vacuo and the residue coevaporated three times with $CHCl_3$ (3 × 3 mL), yielding the desired compound **8** in almost quantitative yields (266 mg, 0.59 mmol) (see Scheme 2).

*Synthesis of tert-Butyl(Monomethoxy)Triethylene Glycol Acetate (**9**).* Monomethoxytriethylene glycol (1.5 g, 9.13 mmol) was dissolved in 6.0 mL of dry THF, and NaH 60% p.p. (730 mg, 18.3 mmol) and then *t*-butyl bromoacetate (3.37 mL, 22.8 mmol) were sequentially added (see Scheme 3). The solution was stirred at room temperature for 12 h, then CH_3OH (1 mL) was added and the solvent removed in vacuo. The crude product, dissolved in $CHCl_3$ and filtered on Celite,

Scheme 2. Synthetic Scheme for the Preparation of Cholesteroxy Acetic Acid (8)[a]

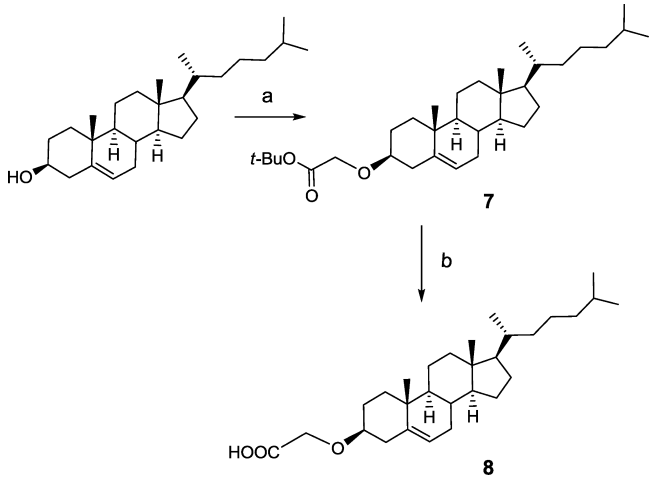

[a]Reaction conditions: (a) NaH, *tert*-butyl bromoacetate, THF, 12 h, r.t.; (b) HCOOH, 2 h, r.t.

Scheme 3. Synthetic Scheme for the Preparation of CH_3O-TEG Acetic Acid (10)[a]

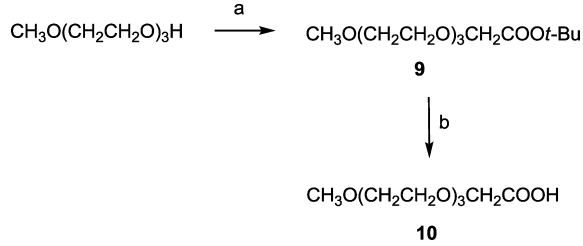

[a]Reaction conditions: (a) NaH, *tert*-butyl bromoacetate, THF, 12 h, r.t.; (b) HCOOH, 2 h, r.t.

was then purified by chromatography on a silica gel column with $CHCl_3$ as eluent, yielding the desired ester **9** in 98% yield (2.5 g, 8.96 mmol).

*Synthesis of (Monomethoxy)Triethylene Glycol Acetic Acid (**10**).* Ester **9** (630 mg, 2.26 mmol) was dissolved in 1.5 mL of formic acid and stirred at room temperature for 2 h (see Scheme 3). The solvent was then removed in vacuo, and the residue was coevaporated three times with $CHCl_3$ (3 × 3 mL), yielding the desired carboxylic acid **10** in 99% yield (500 mg, 2.25 mmol).

*Synthesis of Complex **1** (ToThyCholRu).* **6** (32 mg, 0.033 mmol) was dissolved in 1 mL of dry acetonitrile and then [*trans*-$RuCl_4(DMSO)_2$]$^-$ Na^+ (14 mg, 0.033 mmol) was added. The reaction mixture was stirred at 50 °C and the solvent was then removed in vacuo (see Scheme 1). The reaction, monitored by TLC on alumina, showed in 4 h the total disappearance of **6** to give the desired product **1** in quantitative yields.

*Synthesis of Complex **11** (AziRu).* In analogy to the synthesis of **1**, pyridine (3.0 μL, 0.037 mmol) was dissolved in 0.3 mL of dry acetonitrile and then [trans-$RuCl_4(DMSO)_2$]$^-$ Na^+ (15.6 mg, 0.037 mmol) was added. The reaction mixture was stirred at 50 °C for 2 h and the solvent was then removed in vacuo, giving the desired product AziRu, identified on the basis of its NMR and ESI-MS data (data not shown), in quantitative yields.

dx.doi.org/10.1021/bc200565v | *Bioconjugate Chem.* 2012, 23, 758−770

Lipid-Based Aggregate Preparation. The samples containing ToThyChol and ToThyCholRu were dissolved in a pseudophysiological solution. This latter solution was prepared in double-distilled and degassed water dissolving appropriate amounts of NaCl and KH_2PO_4 so that their final concentrations were 0.140 mol dm^{-3} and 0.010 mol dm^{-3}, respectively. pH was then adjusted to 7.4 by adding appropriate amounts of KOH. This value was checked to be within 0.1 pH units by means of a Radiometer pHM220 pH-meter equipped with a combined glass electrode previously calibrated with IUPAC standard buffer solutions.

For the samples containing POPC and ToThyCholRu, a standard procedure to form vesicles was applied: weighed amounts of ToThyCholRu and POPC were dissolved in chloroform, favoring the process by a slight warming (~40 °C) and sonication treatment (~5 min). Then, the solutions were transferred in round-bottom glass tubes, and a thin film of the solutes was obtained through evaporation of the solvent with dry nitrogen and keeping the samples under vacuum for at least 24 h. The film was then hydrated with H_2O or the pseudophysiological solution.

The vesicle suspensions were slightly heated at 40 °C and sonicated for 15 min at 59 kHz with a FALC LBS2 ultrasonic bath and, finally, repeatedly extruded through polycarbonate membranes of 100 nm pore size, for at least 11 times.

Samples for SANS measurements were prepared in heavy water (D_2O, isotopic enrichment >99.8%, molar mass 20.03 g mol^{-1}) purchased from Aldrich, in order to minimize the incoherent contribution to the scattering cross sections arising from the system. Samples to be analyzed by EPR also included 1% (w/w) of spin-labeled phosphatidylcholine (1-palmitoyl-2-[*n*-(4,4-dimethyloxazolidine-*N*-oxyl)]stearoyl-*sn*-glycero-3-phosphocholine, *n*-PCSL, *n* = 5, 7, 10, 14), purchased from Avanti Polar Lipids and stored at −20 °C in ethanol solutions.

Lipid-Based Aggregate Characterization. The lipid-based aggregate characterization has been achieved by different experimental techniques such as DLS, to get information on particle dimensions; SANS, to reach a deeper insight into the aggregate structure; UV−vis measurements, to evaluate their stability in time; and EPR, to confirm aggregate stability and investigate the membrane microstructure.

Dynamic Light Scattering (DLS). Dynamic light scattering investigations were performed with a setup composed of a Photocor compact goniometer, a SMD 6000 Laser Quantum 50 mW light source operating at 5325 Å, and a PMT-120-OP/B and a correlator (Flex02−01D) purchased from Correlator.com. All the measurements were performed at (25.00 ± 0.05) °C with the temperature controlled through the use of a thermostat bath. In dynamic light scattering, the intensity autocorrelation function $g^{(2)}(t)$ is measured and related to the electric field autocorrelation function $g^{(1)}(t)$ by the Siegert relation[14]

$$g^{(2)}(t) = 1 + \beta |g^{(1)}(t)|^2 \tag{1}$$

where β is the coherence factor, which accounts for the deviation from ideal correlation and depends on the experimental geometry. The function $g^{(1)}(t)$ can be written as the Laplace transform of the distribution of the relaxation rates, Γ, used to calculate the translational diffusion coefficient, D

$$g^{(1)}(t) = \int_{-\infty}^{+\infty} \tau A(\tau) \exp\left(-\frac{t}{\tau}\right) \mathrm{d} \ln \tau \tag{2}$$

where $\tau = 1/\Gamma$. Laplace transforms were performed using a variation of CONTIN algorithm incorporated in *Precision Deconvolve* software. From the relaxation rates, the *z*-average of the diffusion coefficient D may be obtained as follows:[15]

$$D = \lim_{q \to 0} \frac{\Gamma}{q^2} \tag{3}$$

where $q = (4\pi n_0)/(\lambda \sin(\theta/2))$ is the modulus of the scattering vector, n_0 the refractive index of the solution, λ the incident wavelength, and θ the scattering angle. An example of Γ fit vs q^2, to get the slope of the straight line, is shown in Figure S1 of the Supporting Information.

Provided that the solutions are quite dilute, the Stokes−Einstein equation, which rigorously holds at infinite dilution for non-interacting spherical species[16] diffusing in a continuous medium, may legitimately be used to evaluate the hydrodynamic radius R_H of the aggregates:[17,18]

$$R_H = \frac{kT}{6\pi\eta D} \tag{4}$$

where k is the Boltzmann constant, T is the absolute temperature, and η is the medium viscosity. In the case of nonspherical particles, R_H in eq 4 represents the radius of equivalent spherical aggregates with the same diffusion coefficient.

Small-Angle Neutron Scattering (SANS). Small angle neutron scattering measurements were performed at 25 °C with the KWS2 instrument located at the Heinz Maier-Leibnitz neutron source of the Jülich Centre for Neutron Science (Garching, Germany). Neutrons with an average wavelength of 7 Å and 19 Å and a wavelength spread $\Delta\lambda/\lambda \leq 0.2$ were used. A two-dimensional 128 × 128 array scintillation detector at three different wavelength (W)/collimation (C)/sample-to-detector (D) distances ($W_{7Å}C_{8m}D_{8m}$, $W_{7Å}C_{8m}D_{2m}$, and $W_{19Å}C_{8m}D_{8m}$) was used. These configurations allowed collection of data in a range of the scattering vector modulus $q = 4\pi/\lambda \sin(\theta/2)$ located between 0.002 and 0.25 $Å^{-1}$. The obtained raw data were corrected for background and empty cell scattering. Detector efficiency corrections, radial average, and transformation to absolute scattering cross sections were made with a secondary plexiglass standard.[19]

Depending on the scattering intensity profiles, different models were adopted to fit the collected date. For cylindrical aggregates (as in the case of the ToThyCholRu aggregates, see below), the following equation was used:

$$\frac{\mathrm{d}\Sigma}{\mathrm{d}\Omega} = \frac{\phi_{cyl}(1-\phi_{cyl})\pi^2 R^2 \Delta^2 \rho}{q} \exp\left(-\frac{q^2 R^2}{4}\right) + \left(\frac{\mathrm{d}\Sigma}{\mathrm{d}\Omega}\right)_{\mathrm{incoh}} \tag{5}$$

where R is the radius of the base, ϕ_{cyl} the cylinder volume fraction, and $\Delta\rho$ the scattering length density difference between the cylinders and the solvent.

dx.doi.org/10.1021/bc200565v | *Bioconjugate Chem.* 2012, 23, 758−770

In the presence of vesicles, the system was modeled as a collection of unilamellar and multilamellar vesicles:[20]

$$\frac{d\Sigma}{d\Omega} = \frac{1}{q^2}\langle |f(q)|^2\rangle\left(1 + \frac{\langle |f(q)|\rangle^2}{\langle |f(q)|^2\rangle}(S(q) - 1)\right) + \left(\frac{d\Sigma}{d\Omega}\right)_{incoh} \quad (6)$$

In eq 6, $f(q)$ is the form factor of a bilayer containing information on the shape of the scattering objects, whereas $S(q)$ is the structure factor that takes into account the interferences occurring among the bilayers belonging to a single stack of lamellae. $(d\Sigma/d\Omega)_{incoh}$ represents the incoherent contribution to the cross section measured, mainly due to the presence of hydrogenated molecules.

UV–vis Measurements. All the UV–vis measurements were acquired on a Cary Varian 5000 spectrophotometer equipped with a multicell holder. Temperature within the cell was controlled using the Peltier thermocouple. Quartz cuvettes with a path length of 1.0 cm were used for the measurements. Wavelength scans were performed at 25 °C from 200 to 800 nm, with a 300 nm/min scan speed.

Electron Paramagnetic Resonance (EPR). EPR spectra were recorded on a 9 GHz Bruker Elexys E-500 spectrometer (Bruker, Rheinstetten, Germany). Capillaries containing the samples were placed in a standard 4 mm quartz sample tube containing light silicone oil for thermal stability. The temperature of the sample was regulated at 25 °C and maintained constant during measurement by blowing thermostatted nitrogen gas through a quartz Dewar. The instrumental settings were as follows: sweep width, 120 G; resolution, 1024 points; modulation frequency, 100 kHz; modulation amplitude, 1.0 G; time constant, 20.5 ms, incident power, 5.0 mW. Several scans, typically 64, were accumulated to improve the signal-to-noise ratio. Values of the outer hyperfine splitting, $2A_{max}$, were determined by measuring, through a homemade MATLAB-based routine, the difference between the low-field maximum and the high-field minimum. This parameter is a useful empirical measure of the lipid chain dynamics and order in both gel and fluid phases of lipid bilayers.[21,22] The main source of error on the $2A_{max}$ value is the uncertainty in composition of samples prepared by mixing few microliters of mother solutions. For this reason, reproducibility of $2A_{max}$ determination was estimated by evaluating its value for selected independently prepared samples with the same nominal composition. It was found that the uncertainty was ±0.2 G.

Cell Cultures, Proliferation, and Viability. Bioactivity and cytotoxicity of ruthenium-containing nucleolipidic nanoparticles and of AziRu was investigated using a limited panel of human tumor cell lines (HeLa cervical cancer cells, CaCo-2 and WiDr epithelial colorectal adenocarcinoma cells, MCF-7 breast adenocarcinoma cells, SH-SY5Y neuroblastoma cells), all purchased from ATCC (American Type Culture Collection, Manassas, Virginia, USA). Cells were cultured at 37 °C in a humidified 5% CO_2 atmosphere and were grown in Dulbecco's modified Eagle's medium (DMEM, Invitrogen, Paisley, U.K.) containing high glucose (4.5 g/L) or in RPMI medium (Invitrogen, Paisley, U.K.). Media were supplemented with 10% fetal bovine serum (FBS, Cambrex, Verviers, Belgium), L-glutamine (2 mM, Sigma, Milan, Italy), penicillin (100 units/mL, Sigma), and streptomycin (100 μg/mL, Sigma), according to ATCC recommendations. For cytotoxicity studies, cells were washed with PBS buffer solution (Sigma), collected by trypsine (Sigma), and then inoculated in a 96-microwell culture plate at density of 10^4 cells/well. Cells were allowed to grow for 24 h; then, the medium was replaced with fresh medium and cells were treated for a further 72 h with a range of concentrations (25–1000 μM) of (i) AziRu and POPC liposomes, and (ii) of the nucleolipidic aggregates ToThyChol (**6**, Scheme 1), ToThyCholRu (**1**, Scheme 1), and ToThyCholRu/POPC. In more detail, 1 or 2 μL of physiological solutions containing POPC, AziRu, ToThyChol, ToThyCholRu, and ToThyCholRu/POPC were added to cell culture medium to give concentrations ranging from 25 to 1000 μM.

Cell number and proliferation were determined by the trypan blue dye exclusion test. After these treatments, the medium was removed and the cells were washed twice with PBS buffer solution (Sigma) and then incubated with a trypsin–EDTA solution (Sigma) at 37 °C for 5 min. Trypsin was inactivated by resuspending the cells in medium containing 10% FBS (Cambrex). The cells were pelleted at 250*g* and resuspended in PBS. Viable cells, cells that excluded 0.4% trypan blue (Sigma), were then counted with a hemocytometer. Concurrently, cell viability was evaluated with an MTT assay procedure, which measures the level of mitochondrial dehydrogenase activity using the yellow 3-(4,5-dimethyl-2-thiazolyl)-2,5-diphenyl-2*H*-tetrazolium bromide (MTT, Sigma) as substrate.[23] The assay was based on the redox ability of living mitochondria to convert dissolved MTT into insoluble purple formazan. Briefly, after the treatments the medium was removed and the cells were incubated with 20 μL/well of an MTT solution (5 mg/mL) for 1 h in a humidified 5% CO_2 incubator at 37 °C. The incubation was stopped by removing the MTT solution and by adding 100 μL/well of DMSO to solubilize the purple formazan. Finally, the absorbance was monitored at 530 nm by using a multiwell plate reader in a Perkin-Elmer LS 55 Luminescence Spectrometer (Perkin-Elmer Ltd., Beaconsfield, U.K.).[24]

The calculation of the concentration required to inhibit the net increase in the cell number and viability by 50% (IC_{50}) is based on plots of data carried out in triplicate and repeated three times. IC_{50} values were obtained using a dose response curve by nonlinear regression using a curve fitting program, *GraphPad Prism 5.0*, and are expressed as mean ± SEM.

RESULTS AND DISCUSSION

Synthesis. Thymidine-based ruthenium complex **1** (Figure 1*a*)—following the design of a uridine-based system previously described by some of us[6]—was prepared in five straightforward steps as depicted in Scheme 1.

As a privileged ligand for transition metal complexes, one pyridine residue, attached through a methylene linker at the N-3 position of thymidine, was selected to provide the functional group useful for ruthenium trapping. Its insertion on the pyrimidine nucleobase was achieved in almost quantitative yields by treatment of the 5′-DMT protected nucleoside **2** with 4-(bromomethyl)pyridine in DMF using K_2CO_3 as the base (Scheme 1).

In order to obtain the target amphiphilic nucleolipid, the ribosidic hydroxy groups of alkylated nucleoside **3** were conjugated with hydrophilic and lipophilic chains. Ester linkages were chosen to attach these components to hydroxy moieties, and thus obtain effective pro-drugs, on the basis of several advantages. First of all, they can be realized by simple and high-yielding couplings of suitable carboxylic acids; second,

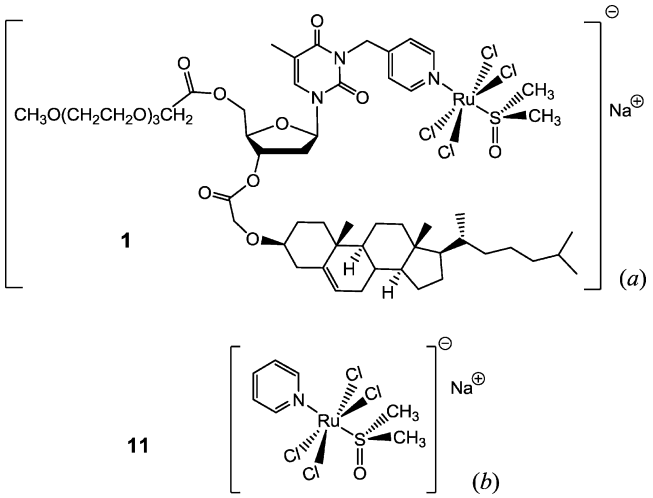

Figure 1. Molecular structure of (*a*): cholesterol-based nucleolipid-ruthenium complex **1** (ToThyCholRu); (*b*) pyridine-based ruthenium complex **11** (AziRu).

esters are stable covalent bonds in neutral and extracellular media, but are easily reversible once inside the cells, being rapidly degraded by esterases.

The desired nucleolipid **6** was synthesized by sequential insertion on **3** of two diverse appendages: one hydrophilic oligo(ethylene glycol) chain at the 5′-OH moiety, and one cholesterol residue, as the lipophilic component, attached at the 3′-OH position.

Cholesterol, selected here as the lipophilic decoration of the target functional nucleolipid in consideration of both its affinity with lipid membrane constituents and its easy availability, was first converted into ester **7** by reaction with *tert*-butyl bromoacetate and NaH in THF, followed by treatment with formic acid, assuring *tert*-butyl removal and recovery of target acid **8** in almost quantitative yields (Scheme 2).

A similar synthetic scheme was adopted to obtain the selected hydrophilic component, i.e., monomethoxy-triethylene glycol (TEG), in the form of carboxylic acid. This oligoether was first converted into *tert*-butyl ester **9**, then subjected to formic acid-promoted cleavage, giving oligoether-derivatized acetic acid **10** (Scheme 3).

Reaction of **3** with cholesterol derivative **8**, first, followed by detritylation and condensation of the resulting **5** with monomethoxy-TEG acetic acid **10**, with both couplings carried out using DCC as the activating agent, led to target nucleolipid **6**. Successive complexation with ruthenium was achieved by mixing **6** with the salt $[\text{trans-RuCl}_4(\text{DMSO})_2]^-\text{Na}^+$, prepared following literature procedures,[25] in CH_3CN at 50 °C for 4 h.

All the intermediate compounds were purified by silica gel column chromatography and characterized by ^{1}H and ^{13}C NMR spectroscopy and MS analysis. Target salt **1**, purified on alumina, was identified by ESI-MS spectrometry in the negative mode, showing m/z values in accordance with the expected mass. More difficult was the NMR characterization of the complex, with the ^{1}H and ^{13}C NMR spectra showing broadened signals, due to the presence of the paramagnetic Ru(III) nucleus. In the ^{1}H NMR spectrum in $CDCl_3$ of salt **1**, this also induced a dramatic upfield shift of the pyridine protons and of the methyl protons of the DMSO ligand, here found at $\delta = -1.87$ ppm and $\delta = -12.66$ ppm, respectively, as very broad signals, which can be considered diagnostic of the effective complex formation.[26,27]

Dynamic Light Scattering (DLS). ToThyChol (**6**, Scheme 1) exhibits a quite high solubility in water (>1−2 mmol/kg) with respect to the almost insoluble pure cholesterol. Furthermore, it shows self-aggregation properties due to its amphiphilic characteristics. DLS measurements carried out on ToThyChol at increasing sample concentration in pseudophysiological conditions reveal the presence of a monomodal radii distribution centered around 150 nm in the whole concentration range studied (see Figure 2 graph *a*). The dimensions of ToThyChol aggregates are shown in SI Table S1.

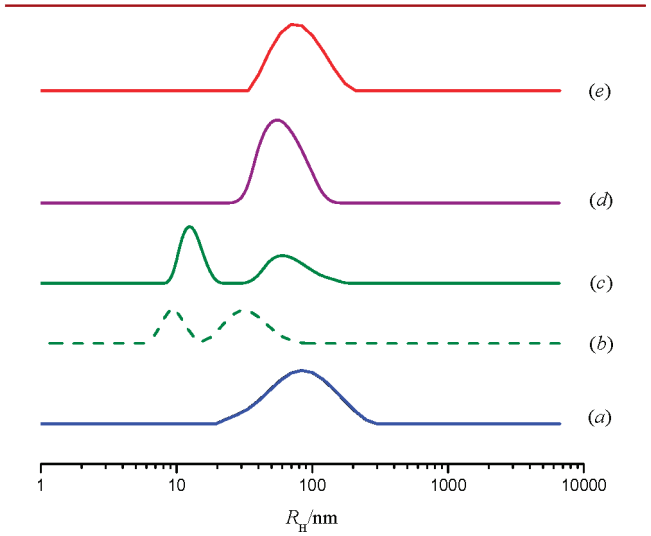

Figure 2. Example of size distribution of the ToThyChol and ToThyCholRu aggregates at 90°: (*a*) ToThyChol in pseudophysiological conditions, (*b*) ToThyCholRu in water, (*c*) ToThyCholRu in pseudophysiological conditions, (*d*) ToThyCholRu-POPC 15:85, (*e*) pure POPC in pseudophysiological conditions.

ToThyCholRu (**1**, Scheme 1) shows ability in nanostructuring, though its stability is limited in time. In fact, depending on the environmental conditions, we observed a clear change of the Ru-complex properties in a few hours (pseudophysiological conditions) or a few days (pure water).

DLS measurements performed on ToThyCholRu fresh solution both in water and in pseudophysiological conditions show a bimodal relaxation time distribution corresponding to the presence of two different aggregates whose mean hydrodynamic radii are ∼10 and ∼30 nm, respectively (see Figure 2 graphs *b*, *c*). However, the aggregate size progressively tends to increase, leading to the formation of small dark particles after 78 h in water and after 4−6 h in pseudophysiological conditions.

UV−vis. As in the case of NAMI-A,[11,12,28] ToThyCholRu complex in aqueous solution also suffers the replacement of its four chloride ligands by hydroxide ions, water molecules, or even buffer components, resulting in degradation of the initial complex. This effect is shown by the time evolution of the UV−vis spectra of ToThyCholRu both in pure water and in pseudophysiological conditions (see Figure 3 *a*, *b*).

Small-Angle Neutron Scattering (SANS). Information on the aggregate structure can be achieved by SANS measurements. The morphology of the aggregates has been obtained by means of small-angle neutron scattering. As shown in Figure 4*a*, the scattering profile of ToThyCholRu in pure heavy water

dx.doi.org/10.1021/bc200565v | *Bioconjugate Chem.* 2012, 23, 758−770

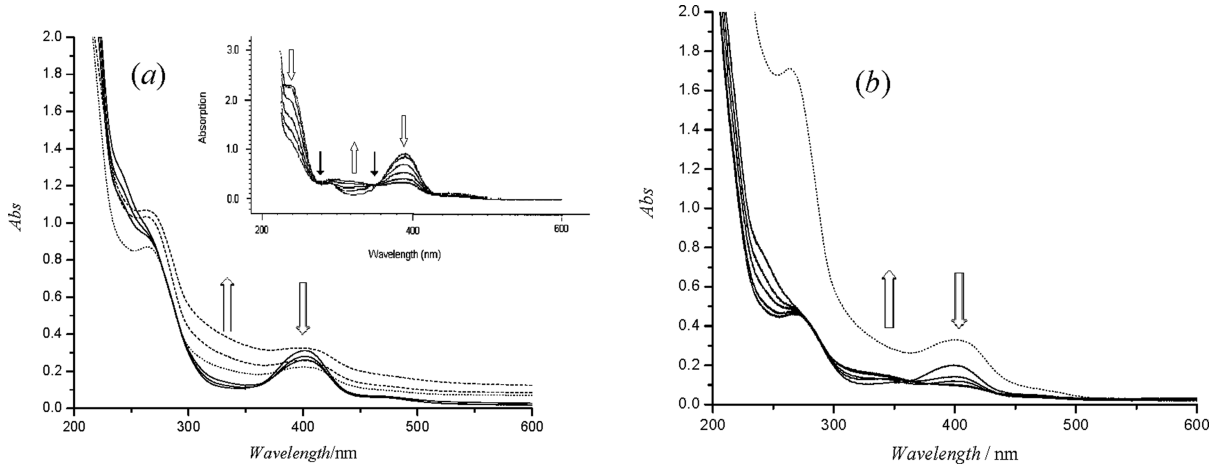

Figure 3. Absorbance evolution with time of 0.1 mmol kg^{-1} ToThyCholRu solution in (*a*) water (72 h), (*b*) pseudophysiological conditions (4 h). Two isosbestic points are present at 274 and 358 nm, respectively. The dashed lines refer to the formation of dark particles in solution, and the arrows indicate the direction of evolution with time. The inset represents the absorbance evolution with time of NAMI-A solution (reproduced with permission of *International Journal of Pharmaceutics*, Elsevier Limited, The Boulevard, Langford Lane Kidlington, Oxford, OX5 1GB, U.K. License number 2757030300954 released on Sep 27, 2011).

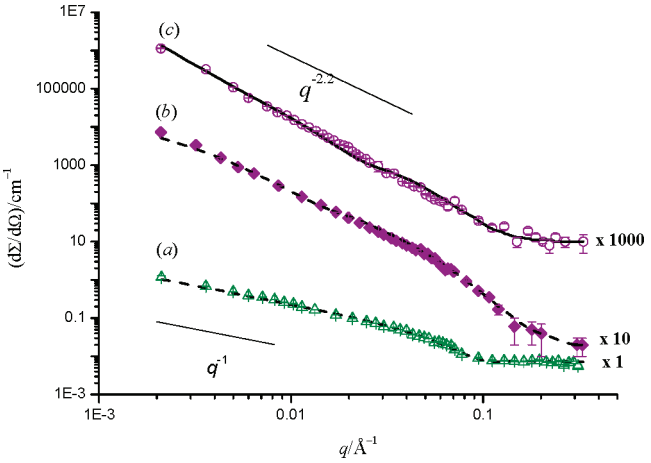

Figure 4. Scattering cross-section profiles for (*a*) ToThyCholRu in pure D_2O, (*b*) ToThyCholRu-POPC 5:95, and (*c*) ToThyCholRu-POPC 15:85 (in pseudophysiological conditions). The curves correspond to the appropriate fit equations. For a better visualization, data have been multiplied by a scale factor, as indicated.

shows a power law decay $d\Sigma/d\Omega \propto q^{-1}$. The slope −1 in a double log representation suggests the presence of cylindrical or near-cylindrical aggregates. Furthermore, this slope is quite constant over a large q range, changing to a −4 value only at high q, as expected in the Porod region.[29] Nevertheless, DLS measurements revealed the presence of two aggregates quite different in size (see Figure 2*b*,*c*).

This different experimental evidence can be matched either by admitting that both aggregates shown by DLS have a cylindrical shape or that the long cylindrical objects detected by SANS dominate in number and in size over the smaller ones. The former interpretation seems unrealistic on the basis of the very low value of the mean hydrodynamic radius (7÷10 nm) of the smaller aggregates. Thus, it appears more reasonable to admit that in the studied system there is coexistence of spherical or almost-spherical objects and long cylinders. In order to clarify this point, we simulated the scattering profile due to the simultaneous contribution to the form factor of spheres and cylinders. The results are shown in Figure S2 of the Supporting Information. The simulation suggests that a quite satisfactory reproduction of the experimental SANS data is only possible by admitting that the cylindrical objects represent more than 99% of the total volume of the aggregates, so that it is likely that in the ToThyCholRu systems the dominating population of aggregates presents a cylindrical shape.

On this basis, the experimental scattering data were modeled through eq 5. Model fit allows the estimation of the micelle radius R that results as (3.1 ± 0.5) nm. Unfortunately, the lack of the Guinier regime[29] in the scattering profile does not provide the possibility to calculate the length of the cylindrical micelles, l. Nonetheless, an estimation of its value can be obtained from the knowledge of the DLS hydrodynamic radius R_H that for a cylinder is given by[30]

$$R_H = \sqrt[3]{\frac{3}{4}R^2 l}\left[1.0304 + 0.0193x + 0.06229x^2 + 0.00476x^3 + 0.00166x^4 + \left(2.66\cdot10^{-7}\right)x^7\right] \quad (7)$$

where $x = \ln[l/(2R)]$ and R is the cylinder radius.

In order to avoid an overestimation of the experimental data, the above equation has been applied only to the larger aggregates in Figure 2. Upon application of eq 7 to ToThyCholRu aggregates, and on the basis of the hydrodynamic radius obtained by DLS, namely, 85−120 nm, it is possible to estimate that the cylinder length ranges between 1000 and 1400 nm.

Stabilization of ToThyCholRu. In order to increase the stability of ToThyCholRu in aqueous solution, the complex was lodged into POPC phospholipid bilayers.

Several samples of the system ToThyCholRu-POPC at different molar ratio (5:95, 10:90, 15:85, 20:80) in pseudophysiological solutions have been prepared, and their evolution with time has been monitored by UV−vis measurements.

As for the pure ToThyCholRu solutions, all the systems were light yellow immediately after preparation, giving superimposable spectra. However, while 5:95, 10:90, and 15:85 samples remained substantially unchanged for weeks, the 20:80 sample turned brown after 5−6 days. An example of the UV−

dx.doi.org/10.1021/bc200565v | *Bioconjugate Chem.* 2012, 23, 758−770

vis spectra over a time of 6 days (150 h) for the 15:85 sample is depicted in Figure 5. The absence of significant changes with

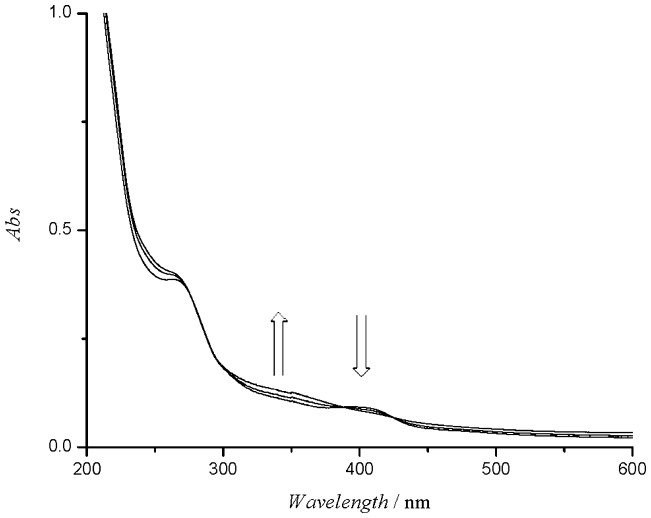

Figure 5. UV−vis time evolution of the ToThyCholRu-POPC 15:85 sample at 0.3 mmol kg^{-1} total concentration in pseudophysiological conditions over a period of 150 h. The arrows indicate the sense of the spectra evolution with time.

time in the spectra is a good indication of the formulation stability; no precipitation was observed as well. Furthermore, neither DLS nor EPR detected substantial changes with time in the aggregate dimensions and bilayer fluidity, as discussed below.

DLS measurements performed on the same 15:85 formulation, both in water and in pseudophysiological conditions, revealed for both systems the presence of aggregates with monomodal distribution having a mean hydrodynamic radius of 60 and 90 nm, respectively (see Figure 2*d*). Their size was invariant with time up to 5−6 days.

From the data obtained through SANS experiments, it was possible to identify the aggregates as liposomes. In fact, as shown in Figure 4*b*,*c*, the scattering profile of ToThyChol-POPC vs q shows slopes with a power law decay, $q^{-\alpha}$, with $\alpha > 2$ both in water and in pseudophysiological conditions. This is typical of bilayer structures that in the present case reflect the presence of liposomes.

It is worth noting that in both profiles the slope α in the intermediate q range is constantly ≥ 2, indicating the absence of coexisting pure ToThyCholRu cylindrical micelles, for which q^{-1} dependence should occur. It is thus possible to conclude that ToThyCholRu is quantitatively inserted in the liposome bilayer.

Since the α exponent is larger than 2, the aggregates were modeled as multilamellar systems (see eq 6). However, α value is only slightly larger than 2, and this is consistent with a small number of lamellae. It is likely that both single lamellar and some multilamellar vesicles are present.

The thickness of the layer changes from ∼4.0 nm for pure POPC liposomes to ∼4.5 nm for ToThyCholRu-POPC (5:95) and to ∼5.0 nm for ToThyCholRu-POPC (15:85) (see Table 1), indicating that the housing of the ToThyCholRu in the bilayer produces a slight increase of its thickness.

Electron Paramagnetic Resonance (EPR). Spin-label EPR spectroscopy has been proven to give substantial information on the acyl chains structuring in the lipid bilayers.[31−34] In this study, different spin-labels were used. They presented a nitroxide group, positioned at the levels of the 5, 7, 10, and 14 carbon atom of a phosphocholine backbone of a *sn*-2 chain, from here on called *n*-PCSL. 5-PCSL bears the radical label close to the molecule headgroup and consequently allows monitoring of the behavior of the region of the membrane inner core closer to the polar external layers. In contrast, 14-PCSL bears the radical label close to the terminal methyl group of the acyl chain, thus giving information on the more internal region of the membrane hydrophobic core. The goal has been to investigate how the membrane microstructure is influenced by the presence of ToThyCholRu at different ToThyCholRu/POPC ratios.

EPR spectra of *n*-PCSL in ToThyCholRu-POPC liposomes at 15:85 molar ratio are shown in Figure 6. In the same figure, the EPR spectra of the spin-labels in pure POPC vesicles are also presented.

For pure POPC, the 5-, 7-, and 10-PCSL spectra present a clearly defined axial anisotropy (see Figure 6, solid lines). In contrast, 14-PCSL spectrum shows an almost isotropic three-line signal, indicative of a rather free motion of the radical label. The higher isotropy of the 14-PCSL spectrum indicates a

Table 1. SANS, UV−vis, and DLS Results on Different ToThyCholRu/POPC Systems[a]

		SANS	UV−vis	DLS	SANS	
solvent	molar ratio	shape	degradation time/h	R_H/nm	lamellae number	layer thickness/nm
			ToThyCholRu			
pseudophys. buffer	100:0	cylinder	–	∼150 ± 15		3.1 ± 0.5 (cylinder radius)
			ToThyCholRu:POPC			
water	100:0	sphere	72	7.4 ± 0.5		
		cylinder		120 ± 30		
pseudophys. conditions	100:0	sphere	4	12 (*)		
		cylinder		85 (*)		
pseudophys. conditions	0:100	vesicles	stable	75 ± 7	1−2	4.0 ± 0.4
water	15:85		stable	64 ± 5		
pseudophys. conditions	5:95	vesicles	stable	78 ± 7	1−2	4.5 ± 0.7
pseudophys. conditions	15:85	vesicles	stable	80 ± 6	1−2	5.0 ± 0.5

[a]Measurements marked with * have been only evaluated at 90°.

dx.doi.org/10.1021/bc200565v | *Bioconjugate Chem.* 2012, 23, 758−770

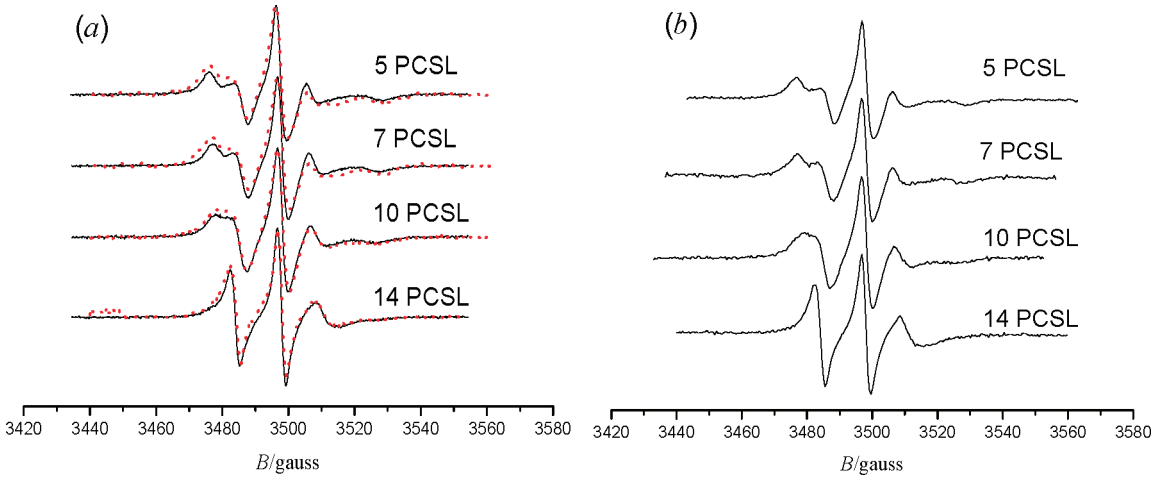

Figure 6. EPR spectra of *n*-PCSL in POPC (continuous line) and in ToThyCholRu/POPC bilayers at the ratio of 15:85 mol/mol (dashed line) freshly prepared (*a*) and ToThyCholRu/POPC bilayers at the molar ratio of 15:85 after 30 days (*b*).

flexibility increase in the segmental chain mobility going from the polar head groups to the inner hydrophobic core, which is a characteristic hallmark of the liquid-crystalline state of fluid phospholipid bilayers.[35]

Spectra of the spin-labels at 15:85 molar ratio in Figure 6, together with the $2A_{max}$ corresponding values in Table 2, show

Table 2. Outer Hyperfine Splitting Parameter $2A_{max}$ of *n*-PCSL in POPC and ToThyCholRu/POPC Liposomes at 25 °C[a]

	ToThyCholRu-POPC					Chol-POPC
	Ru/POPC molar ratio					Chol/POPC molar ratio
n-PCSL	0:100	5:95	10:95	15:85	20:80	20:80
	$2A_{max}$/G					
5-PCSL	52.4	52.7	53.1	53.2	54.0	53.4
7-PCSL	50.6	50.7	51.2	51.4	51.9	51.7
10-PCSL	47.2	46.7	46.1	45.5	45.9	48.5
14-PCSL	33.1	33.4	33.6	33.4	33.5	34.9

[a]The error on $2A_{max}$ value is ±0.2 G.

that the presence of ToThyCholRu complex induces a stiffening effect on the acyl carbon atoms closer to the hydrophilic region of the complex as shown by the increased value of $2A_{max}$ of 5-and 7-PCSL. An opposite effect, connected with an increased fluidity of the membrane, is observed for 10-PCSL. In the case of 14-PCSL, the fluidity of the more hydrophobic region of the bilayer explored by this spin-label is almost invariant. This complex behavior can be rationalized admitting that the presence of a cholesterol moiety at C5 and C7 vicinity creates more room at the level of the inner carbon atom C10 that is not directly interested in the aliphatic chain-cholesterol interaction, thus increasing the local segmental mobility of the acyl chains, while for C14, the presence of the Ru complex is ineffective.

Thus, the experimental results are a clear indication of the perturbation caused by the presence of ToThyCholRu in the phospholipid bilayers, which induces an increase in lipid packing density of the more external acyl chain segments ($n \leq 7$) and enhanced fluidity of the inner chains region ($n \geq 10$). It is interesting to note that pure cholesterol reduces dynamics and increases order of the whole lipid acyl chains in POPC bilayers, as indicated by the $2A_{max}$ values reported in Table 2 (Chol-POPC column). This effect could probably be due to the headgroup of ToThyCholRu, which causes a more intense change in the lipid packing density than that caused by cholesterol, such as to affect the acyl chain mobility.

EPR measurements were repeated several times over a period of 30 days obtaining substantial reproducibility of the results. No degradation was observed for all the samples up to 15:85 molar ratio. An example of the invariance of the EPR spectra with time is reported in Figure 6*b*.

In Vitro Bioactivity Study. We first analyzed the effect on the cell viability of cholesterol-based nucleolipidic nanoaggregates by culturing a panel of human tumor cell lines (HeLa cervical cancer cells, CaCo-2 and WiDr epithelial colorectal adenocarcinoma cells, MCF-7 breast adenocarcinoma cells, SH-SY5Y neuroblastoma cells). As shown in panels A and C of Figure 7 with respect to MCF-7 and WiDr cell lines after 72 h of incubation, ToThyChol did not exhibit a significant cytotoxic effect. The cell viability was also determined in the presence of conventional POPC liposomes, currently used in a broad range of biotechnological applications.[36] As expected, POPC liposomes did not induce cell growth inhibition at all the concentrations and time intervals tested. Substantially, ToThyChol showed little if any divergence compared to POPC liposomes. In this way, as demonstrated by parallel biochemical and toxicological investigations, we can assume that the cholesterol-containing nucleolipidic technological platform ToThyChol is a safe precursor potentially useful for drug delivery applications. Consequently, we further investigated the conversion of ToThyChol aggregates into Ru(III) complexes (ToThyChol-Ru), as such or lodged in the biomimetic membrane formed by the lipid POPC (ToThyCholRu/POPC). To gain an insight into the antiproliferative activity of this novel cholesterol-based nucleolipid–ruthenium complex, its cytotoxicity profile toward human cancer cells was compared to that of a NAMI-A-like ruthenium complex, named AziRu and prepared here for a direct evaluation of their antiproliferative activity. Cell lines were exposed to AziRu for 72 h in a growth inhibition assay, and the cytotoxicity was determined in terms of IC_{50} values. The detected cytotoxicities were rather moderate, and the IC_{50} values for AziRu were 900, 690, 515, 405, and 1500 μM in HeLa, CaCo-2, WiDr, MCF-7, and SH-SY5Y cells, respectively.

dx.doi.org/10.1021/bc200565v | *Bioconjugate Chem.* 2012, 23, 758–770

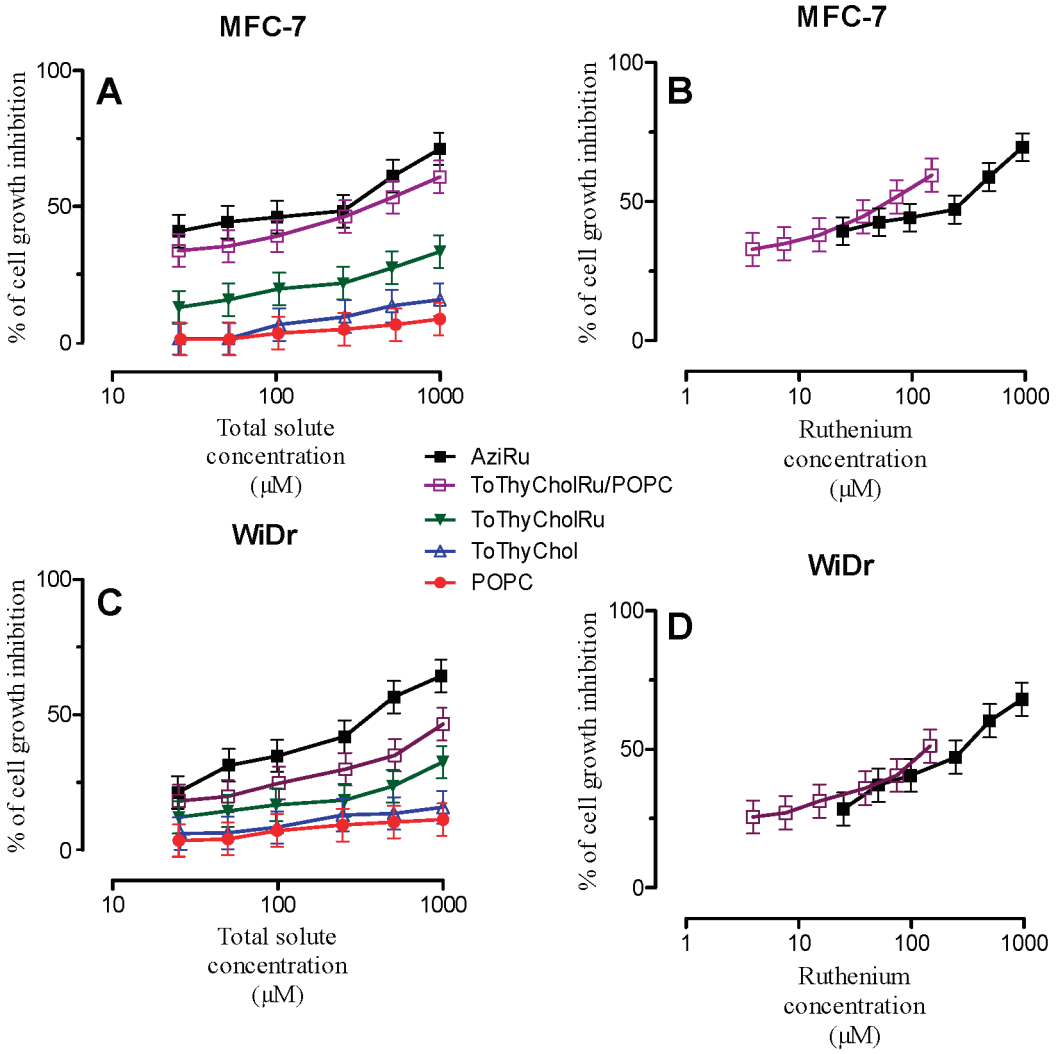

Figure 7. Growth inhibition of MCF-7 (panel A) and WiDr cells (panel C) treated for 72 h with different formulations and with AziRu as indicated in the legend, evaluated by MTT assay and cell counting. In panels B and D, for MCF-7 and WiDr cells, respectively, are reported the corresponding concentration–effect curves obtained by normalizing for the actual amount of ruthenium contained within the ToThyCholRu/POPC liposome. Data are expressed as percentage of untreated cells and are reported as mean of three independent experiments ± SEM.

First, under the same incubation conditions these results indicate a significant difference in ruthenium cytotoxicity exclusively depending on the cell line, suggestive of a selective cell-dependent mechanism of action.[37] Moreover, according to many published studies on ruthenium complexes, our results also showed that AziRu cytotoxicity was much lower than that of a well-known reference drug based on transition metals as the antitumor Cisplatin.[38] However, concerning NAMI-A, it should be considered that the concentration needed to reach cytotoxicity *in vitro* is much higher than the NAMI-A concentration capable of inhibiting the formation of metastases, suggesting that the recognized anti-metastatic activity of NAMI-A is probably not due exclusively to a reduction in cell viability.[39]

Then, focusing on the more sensitive cells (MCF-7 and WiDr lines) to ruthenium action in our *in vitro* experimental model, we assessed the potential cytotoxic effect of ruthenium-containing liposomes, and interestingly, we found that ToThyCholRu/POPC liposome, even if containing only 15 mol % of ruthenium, was able to induce cell growth inhibition in a similar manner to that induced by the same concentrations of AziRu. In other words, the same cytotoxicity shown by AziRu is reached at a ruthenium concentration ~6 times smaller if the metal is lodged in POPC liposomes. In particular, in MCF-7 cells ToThyCholRu/POPC the concentration–response curve was virtually identical to that of AziRu (Figure 7 panel A). Moreover, as reported in panels B and D of Figure 7, by normalizing concentration–effect curves for the actual amount of ruthenium contained within the liposomes, we found that ToThyCholRu/POPC was more active than AziRu in both cell lines. The latter is a noteworthy finding in the design and biological evaluation of innovative supramolecular systems for vectorization of the anticancer drugs. The calculated IC_{50} values reported in Table 3 for the real amount of ruthenium delivered to cells after 72 h of incubation in cell culture media also suggested that the ToThyCholRu/POPC complex was more effective than AziRu in inducing growth inhibition in MCF-7 and WiDr cell lines. In addition, evaluation of the potentiating factor (PF) values demonstrated that ruthenium vectorization by this liposome potentiated the growth inhibition induced by AziRu, reaching values higher than 3 in cancer cells of different histogenesis (see Table 3).

Similar *in vitro* results emerged from bioassays on other human cancer cell lines (data reported in the Supporting

dx.doi.org/10.1021/bc200565v | *Bioconjugate Chem.* 2012, 23, 758–770

Table 3. IC_{50} Values of AziRu (a NAMI-A-like Ru Complex) and of ToThyCholRu/POPC Liposome in the Indicated Cell Lines Following 72 h of Incubation, And Potentiating Factors (P.F.) of ToThyCholRu/POPC

	IC_{50}[a]/μM		P.F.[b]
cell lines	AziRu	ToThyCholRu/POPC	ToThyCholRu/POPC
MCF-7	405 ± 10	70 ± 12	5.7
WiDr	515 ± 15	165 ± 10	3.1

[a]IC_{50} values are reported as mean ± SEM. [b]Potentiating factor calculated as the ratio of IC_{50} values of ToThyCholRu/POPC complex to the IC_{50} of AziRu complex.

Information), albeit generally less sensitive to the action of the antiproliferative ruthenium.

Hence, consistent with our recent report,[40] different aggregate compositions differentially impacts cell viability. As demonstrated by a cytotoxic effect higher than that of AziRu, the cholesterol containing nucleolipidic liposome stabilized with POPC seems to deliver the ruthenium within the cells in a very effective way. Within this context, it is believed that free ruthenium complexes such as NAMI-A enter cells via a passive or facilitated passive transport molecular mechanism, albeit apparently with more difficulty than other antitumor drugs based on transition metal such as Cisplatin.[41] Together with other considerations, this outcome may account for the lower cytotoxicity of emerging ruthenium-based molecules assayed for antineoplastic activity, thus emphasizing the critical role of a proper vehiculation. The importance of liposome stabilization by the presence of the naturally occurring POPC is also supported by the fact that ToThyCholRu liposome per se resulted in a significantly lower cytotoxic effect. In fact, the absence of POPC within these novel liposomal formulations always reduces the effectiveness of the vehiculated anticancer drug. In addition, stable liposome formulations can probably more easily merge with target cell membranes, where the presence of sterols and of other typical membrane constituents might together play a crucial role in both liposome stability and its affinity for cell membranes.

CONCLUSIONS

Herein, we report on a novel cholesterol-based nucleolipidic ruthenium complex stabilized by lipid-based aggregates for antineoplastic therapy. This work was aimed toward the optimization of long-lived nanoaggregates containing high amount of ruthenium complex.

This paper presents the synthesis and assembly properties of the molecules settled, in the "bottom-up" engineering process of the proposed nanovectors. Using thymidine as the central, polyfunctional scaffold, a pyridine-methyl arm was introduced on the nucleobase as a functional ligand able to form an octaedric complex with Ru(III) ion. Insertion of one oligo-(ethylene glycol) chain and one cholesterol residue on the ribosidic moiety confers the desired amphiphilic behavior to this nucleolipid in aqueous solution. The role of the cholesterol moiety, inserted at the level of the sugar ring, is to favor the inclusion of the polyfunctional molecule inside the POPC liposome bilayer thus protecting the Ru complex from degradation. A qualitative picture of the structure of the ruthenium-cholesterol lipid vectors is depicted in Figure 8. Moreover, the presence of the cholesterol residue within the thymidine-based nucleolipidic ruthenium complex gives rise to a safe precursor that results in an attractive platform with useful

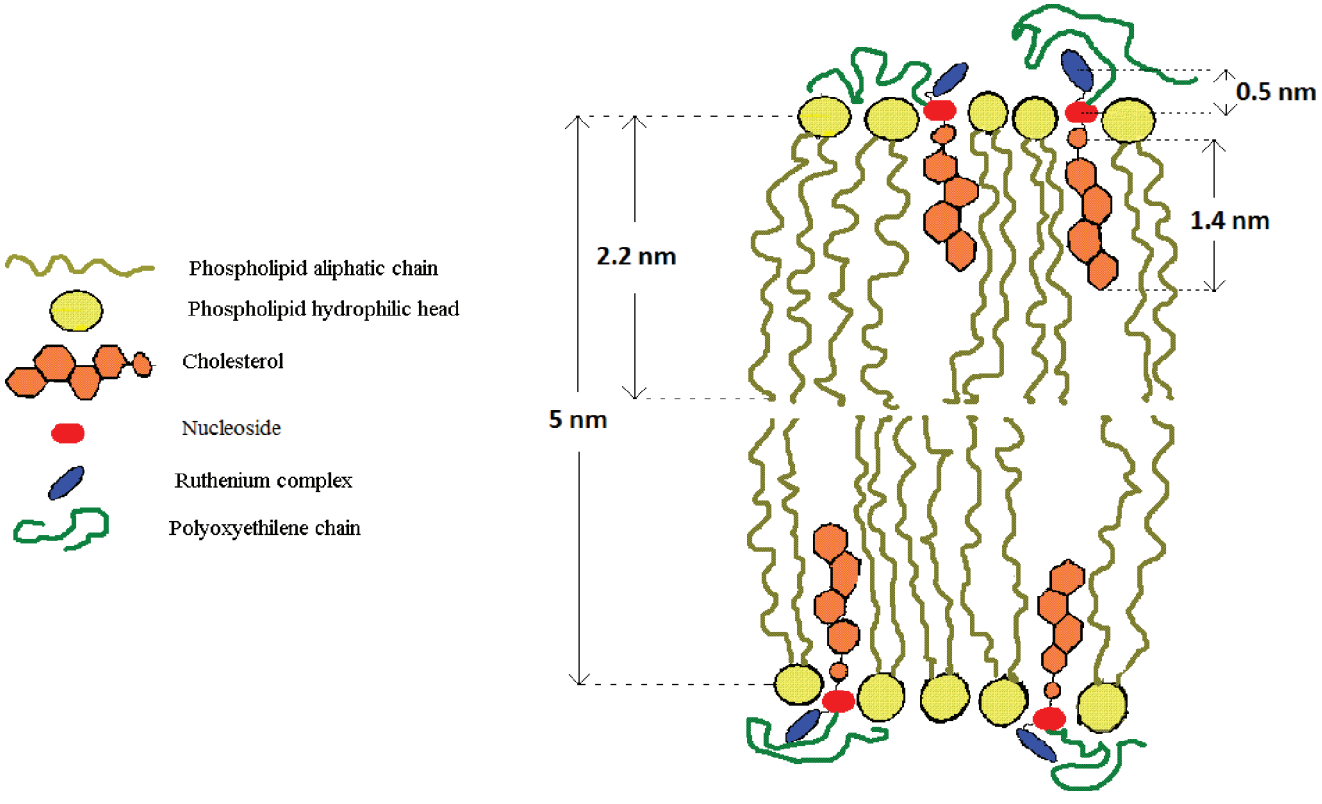

Figure 8. Qualitative graphical representation of ToThyCholRu lodged into a bilayer with indication of some structural parameters.

dx.doi.org/10.1021/bc200565v | *Bioconjugate Chem.* 2012, 23, 758–770

biotechnological features such as molecular carrier abilities for potential applications in drug delivery.

A detailed study of the aggregation behavior has shown that the synthesized compound forms a wide variety of supramolecular aggregates, spanning from spheres and cylinders to oligolamellar vesicles. Aggregates formed only by the Ru-based complex show a degradation kinetics that, depending on pH, is almost complete from a few hours to days, as reported for NAMI-A. However, when the ruthenium complex is lodged in POPC liposomes up to 15 mol %, the degradation is markedly reduced and the formulation is stable for at least several weeks. According to the experimental data, the lipophilic cholesterol residue of ToThyCholRu is lodged well inside the bilayer in the typical position observed for pure cholesterol; meanwhile, the ruthenium is hidden among the phospholipid heads.

It is worth mentioning that *in vitro* bioscreenings based on the evaluation of concentration−effect curves reveal that ToThyCholRu/POPC liposomes are more effective in inhibiting the growth of human cancer cells of different histogenesis with respect to the reference ruthenium-complex NAMI-A-like AziRu. Therefore, this study introduces new perspectives in the synthesis and formulation of highly biocompatible transition-metal-based aggregates having potential application as antineoplastic agents.

■ ASSOCIATED CONTENT

Supporting Information

Molecular characterization of ToThyColRu and its synthesis intermediates, along with supplementary DLS and antiproliferative activity plots,is provided in a separate file. This material is available free of charge via the Internet at http://pubs.acs.org.

■ AUTHOR INFORMATION

Corresponding Author

*E-mail: luigi.paduano@unina.it. Tel. +39 081 674250. Fax. +39 081 674090. E-mail: daniela.montesarchio@unina.it. Tel. +39 081 674126.

Notes

The authors declare no competing financial interest.

■ ACKNOWLEDGMENTS

Project has been funded by MIUR (PRIN 2008 - prot. 20087K9A2J). We thank Forschungszentrum Jülich for provision of beam time. The SANS experiments were supported by the European Commission, NMI3 contract RII3-CT-2003-505925.

■ ABBREVIATIONS

AcOEt, ethyl acetate; Chol, cholesteryl residue; DCC, *N,N*-dicyclohexylcarbodiimide; DCM, dichloromethane; DMAP, 4-(*N,N*-dimethylamino)-pyridine; DMF, *N,N*-dimethylformamide; DMT, 4,4′-dimethoxytriphenylmethyl; Py, pyridine; r.t., room temperature; *t*-Bu, *tert*-butyl; TEA, triethylamine; TEG, triethylene glycol; THF, tetrahydrofuran; Thy, thymidine residue; SANS, small angle neutron scattering; DLS, dynamic light scattering; EPR, electron paramagnetic spectroscopy

■ REFERENCES

(1) Levina, A., Mitra, A., and Lay, P. A. (2009) Recent developments in ruthenium anticancer drugs. *Metallomics 1*, 458−470.

(2) Ryu, M.-H., and Kang, Y.-K. (2009) ML17032 trial: capecitabine/Cisplatin versus 5-fluorouracil/Cisplatin as first-line therapy in advanced gastric cancer. *Expert Rev. Anticancer Ther. 9*, 1745−1751.

(3) Saloustros, E., and Georgoulias, V. (2008) Docetaxel in the treatment of advanced non-small-cell lung cancer. *Expert Rev. Anticancer Ther. 8*, 1207−1222.

(4) Rafique, S., Idrees, M., Nasim, A., Akbar, H., and Athar, A. (2010) Transition metal complexes as potential therapeutic agents. *Biotechnol. Mol. Biol. Rev. 5*, 38−45.

(5) Groessl, M., Tsybin, Y. O., Hartinger, C. G., Keppler, B. K., and Dyson, P. J. (2010) Ruthenium versus platinum: interactions of anticancer metallodrugs with duplex oligonucleotides characterised by electrospray ionisation mass spectrometry. *J. Biol. Inorg. Chem. 15*, 677−688.

(6) Vaccaro, M., Del Litto, R., Mangiapia, G., Carnerup, A. M., D'Errico, G., Ruffo, F., and Paduano, L. (2009) Lipid based nanovectors containing ruthenium complexes: a potential route in cancer therapy. *Chem. Commun. (Cambridge, U.K.)*, 1404−1406.

(7) Mangiapia, G., Vaccaro, M., D'Errico, G., Frielinghaus, H., Radulescu, A., Pipich, V., Carnerup, A. M., and Paduano, L. (2011) Cubosomes for ruthenium complex delivery: formulation and characterization. *Soft Matter. 7*, 10577−10580.

(8) Mangiapia, G., D'Errico, G., Simeone, L., Irace, C., Radulescu, A., Di Pascale, A., Colonna, A., Montesarchio, D., and Paduano, L. (2012) Ruthenium-based complex nanocarriers for Cancer Therapy. *Biomaterials 33*, 3770−3782.

(9) Bijsterbosch, M. K., Rump, E. T., De Vrueh, R. L. A., Dorland, R., Van Veghel, R., Tivel, K. L., Biessen, E. A. L., Van Berkel, T. J. C., and Manoharan, M. (2000) Modulation of plasma protein binding and *in vivo* liver cell uptake of phosphorothioate oligodeoxynucleotides by cholesterol conjugation. *Nucleic Acids Res. 28*, 2717−2725.

(10) Krieg, A. M., Tonkinson, J., Matson, S., Zhao, Q., Saxon, M., Zhang, L. M., Bhanja, U., Yakubov, L., and Stein, C. A. (1993) Modification of antisense phosphodiester oligodeoxynucleotides by a 5′ cholesteryl moiety increases cellular association and improves efficacy. *Proc. Natl. Acad. Sci. U.S.A. 90*, 1048−52.

(11) Mestroni, G., Alessio, E., Sava, G., Pacor, S., Coluccia, M., and Boccarelli, A. (1994) Water-soluble ruthenium(III)-dimethylsulfoxide complexes: chemical behavior and pharmaceutical properties. *Metal-Based Drugs 1*, 41−63.

(12) Sava, G., Alessio, E., Bergamo, A., and Mestroni, G. (1999) Sulfoxide ruthenium complexes: non-toxic tools for the selective treatment of solid tumor metastases. *Topics Biol. Inorg. Chem. 1*, 143−169.

(13) Bacac, M., Hotze, A. C. G., van der Schilden, K., Haasnoot, J. G., Pacor, S., Alessio, E., Sava, G., and Reedijk, J. (2004) The hydrolysis of the anti-cancer ruthenium complex NAMI-A affects its DNA binding and antimetastatic activity: an NMR evaluation. *J. Inorg. Biochem. 98*, 402−412.

(14) Berne, B. J., and Pecora, R. (1975) *Dynamic Light Scattering: with Applications to Chemistry, Biology, and Physics*

(15) Brehm, G. A., and Bloomfield, V. A. (1975) Analysis of polydispersity in polymer solutions by inelastic laser light scattering. *Macromolecules 8*, 663−5.

(16) Paduano, L., Sartorio, R., and Vitagliano, V. (1998) Diffusion Coefficients of the Ternary System α-Cyclodextrin-Sodium Benzenesulfonate-Water at 25 °C: The Effect of Chemical Equilibrium and Complex Formation on the Diffusion Coefficients of a Ternary System. *J. Phys. Chem. B 102*, 5023−5028.

(17) Vaccaro, M., Accardo, A., Tesauro, D., Mangiapia, G., Loef, D., Schillen, K., Soederman, O., Morelli, G., and Paduano, L. (2006) Supramolecular Aggregates of Amphiphilic Gadolinium Complexes as Blood Pool MRI/MRA Contrast Agents: Physicochemical Characterization. *Langmuir 22*, 6635−6643.

(18) Vergara, A., Paduano, L., and Sartorio, R. (2001) Multicomponent Diffusion in Systems Containing Molecules of Different Size. 4. Mutual Diffusion in the Ternary System Tetra(ethylene glycol)-Di(ethylene glycol)-Water. *J. Phys. Chem. B 105*, 328−334.

(19) Wignall, G. D., and Bates, F. S. (1987) Absolute calibration of small-angle neutron scattering data. *J. Appl. Crystallogr. 20*, 28−40.
(20) Kotlarchyk, M., and Ritzau, S. M. (1991) Paracrystal model of the high-temperature lamellar phase of a ternary microemulsion system. *J. Appl. Crystallogr. 24*, 753−8.
(21) Schorn, K., and Marsh, D. (1996) Lipid chain dynamics and molecular location of diacylglycerol in hydrated binary mixtures with phosphatidylcholine: spin label ESR studies. [Erratum to document cited in CA124:196780]. *Biochemistry 35*, 9286.
(22) D'Errico, G., Vitiello, G., Ortona, O., Tedeschi, A., Ramunno, A., and D'Ursi, A. M. (2008) Interaction between Alzheimer's Abeta (25−35) peptide and phospholipid bilayers: The role of cholesterol. *Biochim. Biophys. Acta, Biomembranes 1778*, 2710−2716.
(23) Hansen, M. B., Nielsen, S. E., and Berg, K. (1989) Re-examination and further development of a precise and rapid dye method for measuring cell growth/cell kill. *J. Immunol. Methods 119*, 203−10.
(24) Santamaria, R., Fiorito, F., Irace, C., De Martino, L., Maffettone, C., Granato, G. E., Di Pascale, A., Iovane, V., Pagnini, U., and Colonna, A. (2011) 2,3,7,8-Tetrachlorodibenzo-p-dioxin impairs iron homeostasis by modulating iron-related proteins expression and increasing the labile iron pool in mammalian cells. *Biochim. Biophys. Acta 1813*, 704−12.
(25) Alessio, E., Balducci, G., Calligaris, M., Costa, G., Attia, W. M., and Mestroni, G. (1991) Synthesis, molecular structure, and chemical behavior of hydrogen trans-bis(dimethyl sulfoxide)-tetrachlororuthenate(III) and mer-trichlorotris(dimethyl sulfoxide)-ruthenium(III): the first fully characterized chloride-dimethyl sulfoxide-ruthenium(III) complexes. *Inorg. Chem. 30*, 609−18.
(26) Mestroni, G., Alessio, E., and Sava, G. (1998) New salts of anionic complexes of Ru(III), as antimetastatic and antineoplastic agents, 1997-EP3401; 9800431
(27) Velders, A. H., Bergamo, A., Alessio, E., Zangrando, E., Haasnoot, J. G., Casarsa, C., Cocchietto, M., Zorzet, S., and Sava, G. (2004) Synthesis and Chemical-Pharmacological Characterization of the Antimetastatic NAMI-A-Type Ru(III) Complexes (Hdmtp)[trans-RuCl4(dmso-S)(dmtp)], (Na)[trans-RuCl4(dmso-S)(dmtp)], and [mer-RuCl3(H2O)(dmso-S)(dmtp)] (dmtp = 5,7-Dimethyl[1,2,4]-triazolo[1,5-a]pyrimidine). *J. Med. Chem. 47*, 1110−1121.
(28) Bouma, M., Nuijen, B., Jansen, M. T., Sava, G., Flaibani, A., Bult, A., and Beijnen, J. H. (2002) A kinetic study of the chemical stability of the antimetastatic ruthenium complex NAMI-A. *Int. J. Pharm. 248*, 239−246.
(29) Brumberger, H. (1967) *Small-Angle X-Ray Scattering*, Gordon & Breach, New York.
(30) Hansen, S. (2004) Translational friction coefficients for cylinders of arbitrary axial ratios estimated by Monte Carlo simulation. *J. Chem. Phys. 121*, 9111−9115.
(31) D'Errico, G., Silipo, A., Mangiapia, G., Vitiello, G., Radulescu, A., Molinaro, A., Lanzetta, R., and Paduano, L. (2010) Characterization of liposomes formed by lipopolysaccharides from Burkholderia cenocepacia, Burkholderia multivorans and Agrobacterium tumefaciens: from the molecular structure to the aggregate architecture. *Phys. Chem. Chem. Phys. 12*, 13574−13585.
(32) Lange, A., Marsh, D., Wassmer, K. H., Meier, P., and Kothe, G. (1985) Electron spin resonance study of phospholipid membranes employing a comprehensive line-shape model. *Biochemistry 24*, 4383−92.
(33) Marsh, D. (2010) Structural and thermodynamic determinants of chain-melting transition temperatures for phospholipid and glycolipids membranes. *Biochim. Biophys. Acta 1798*, 40−51.
(34) Moser, M., Marsh, D., Meier, P., Wassmer, K. H., and Kothe, G. (1989) Chain configuration and flexibility gradient in phospholipid membranes. Comparison between spin-label electron spin resonance and deuteron nuclear magnetic resonance, and identification of new conformations. *Biophys. J. 55*, 111−23.
(35) D'Errico, G., D'Ursi, A. M., and Marsh, D. (2008) Interaction of a Peptide Derived from Glycoprotein gp36 of Feline Immunodeficiency Virus and Its Lipoylated Analogue with Phospholipid Membranes. *Biochemistry 47*, 5317−5327.
(36) Walde, P., and Ichikawa, S. (2001) Enzymes inside lipid vesicles: preparation, reactivity and applications. *Biomol. Eng. 18*, 143−177.
(37) Sava, G., Pacor, S., Bregant, F., Ceschia, V., and Mestroni, G. (1990) Metal complexes of ruthenium: antineoplastic properties and perspectives. *Anti-Cancer Drugs 1*, 99−108.
(38) Pluim, D., van Waardenburg Robert, C. A. M., Beijnen Jos, H., and Schellens Jan, H. M. (2004) Cytotoxicity of the organic ruthenium anticancer drug Nami-A is correlated with DNA binding in four different human tumor cell lines. *Cancer Chemother. Pharmacol. 54*, 71−8.
(39) Sava, G., Clerici, K., Capozzi, I., Cocchietto, M., Gagliardi, R., Alessio, E., Mestroni, G., and Perbellini, A. (1999) Reduction of lung metastasis by IMH[trans-RuCl4(DMSO)Im]: mechanism of the selective action investigated on mouse tumors. *Anti-Cancer Drugs 10*, 129−138.
(40) Simeone, L., Mangiapia, G., Irace, C., Di Pascale, A., Colonna, A., Ortona, O., De Napoli, L., Montesarchio, D., and Paduano, L. (2011) Nucleolipid nanovectors as molecular carriers for potential applications in drug delivery. *Mol. BioSyst. 7*, 3075−86.
(41) Bergamo, A., Zorzet, S., Cocchietto, M., Carotenuto, M. E., Magnarin, M., and Sava, G. (2001) Tumour cell uptake G2-M accumulation and cytotoxicity of NAMI-A on TS/A adenocarcinoma cells. *Anticancer Res. 21*, 1893−1898.